Temperature induced color change in gold nanoparticle arrays: Investigating the annealing effect on the localized surface plasmon resonance

Vårin R. A. Holm,[a] Martin M. Greve, and Bodil Holst
Department of Physics and Technology, University of Bergen, Allegaten 55, 5007 Bergen, Norway

(Received 23 June 2016; accepted 7 September 2016; published 27 September 2016)

The localized surface plasmon resonance (LSPR) effect in metal nanoparticles is important for a range of applications, including photovoltaics and sensors. The actual LSPR effect is difficult to predict, because it can vary strongly with the size, shape, surface structure, and surrounding media of the nanoparticles. In order to understand this better, more experimental data are needed. Here, the authors present a study of the LSPR effect in macroscopic two-dimensional square arrays of gold nanoparticles, 50–80 nm in diameter with a pitch of approximately 160 nm, fabricated on borosilicate substrates. The arrays were exposed to different annealing temperatures in steps of 50 up to 600 °C. The authors observe an irreversible blue-shift of the LSPR extinction peak, from around 580 to around 520 nm at annealing temperatures of only 450 °C, an effect clearly visible to the naked eye. The authors also present measurements of the shape of the nanoparticles at the different annealing steps. These measurements were obtained using a combination of scanning electron microscopy (SEM) and atomic force microscopy (AFM). A carefully indexed pattern allowed us to measure the exact same nanoparticles with separate AFM and SEM instruments. The only clear effect that can be observed is that the nanoparticles appear to get smoother with annealing. Our results demonstrate that seemingly minor changes in the metal nanoparticle appearance can lead to a strong change in the LSPR effect. Our results also open up for potential applications in temperature sensing. The fact that the effect of temperature exposure can be observed with the naked eye without any need of electronic readout or power supply is particularly advantageous.
 [http://dx.doi.org/10.1116/1.4963153]

I. INTRODUCTION

A metal nanoparticle (MNP) is smaller than the wavelength of visible light. If the nanoparticle is small enough, the electric field in the incoming light will act uniformly over the whole nanoparticle, displacing the electrons. Combined with the restoring force of the atom cores, this system can be described as an oscillator with a resonance frequency.[1] This effect is referred to as the localized surface plasmon resonance (LSPR) effect, and the macroscopic color of a MNP is determined by the wavelength at which the resonances occur. Varying the shape, size, material, and surrounding medium of the nanoparticles will result in different resonance frequencies. The shape and dielectric function may in turn be affected by external effects applied postfabrication, such as annealing.

There are some investigations on the effect of annealing of nanoparticles of various materials.[2–7] Cai *et al.*[8] reports first a blue-shift and then a red-shift of the absorption peak when annealing 3–5 nm sized silver nanoparticles dispersed within the pores of monolithic mesoporous silica, at temperatures between 500 and 800 °C. Bi *et al.*[9] demonstrate that by alternate annealing in air and H_2, silver nanoparticles dispersed within pores of monolithic mesoporous silica change color. This is attributed to a redox of the Ag nanoparticles, and the process is reversible. Oxidation is not likely to be an issue when annealing gold. Annealing can cause nanoparticles to sink into a glass substrate as reported by Karakouz *et al.*[10] This would mean that a larger portion of the nanoparticle will be surrounded by the substrate rather than air, changing the dielectric function of the surrounding medium and leading to an increase in the refractive index. The quasistatic approximation description of the interaction between a nanoparticle and an electromagnetic field predicts the position of the LSPR to depend on the dielectric function of the surrounding medium[1] so that we would expect a red-shift, should the nanoparticles sink into the substrate. This is assuming that there are no structural changes to the nanoparticles. Bae *et al.*[11] and Jensen *et al.*[12] reports a red-shift for a decrease in nanoparticle height.

Hulteen *et al.*[13] observe a blue-shift when annealing gold nanoparticles located within the 45 nm sized pores of porous alumina membranes up to 400 °C. They present TEM images which shows that the gold nanoparticles goes from being irregular to becoming denser and more uniform, especially the smaller ones. Kessentini *et al.*[14] have investigated the effect of surface roughness on the LSPR, theoretically. They predict a blue shift of approximately 25 nm, for a cylinder with 50 nm diameter and 20 nm height, and a surface root mean square roughness going from 1.6 to 0 nm. Qian *et al.*[15] calculate theoretically that the extinction spectrum blue shift for hollow gold cubes when the corners are rounded. Liu *et al.*[16] show the same for bipyramids when the tips are rounded using finite-difference time-domain (FDTD) simulations; the absorption peak is shifted 40 nm by a change in the radius of curvature from 4.4 to 2.0 nm. All of these examples demonstrate that a change in shape, even a really small, subtle change, can affect the extinction peak significantly.

[a]Electronic mail: varin.andvik@uib.no

Here, we present an experimental study of the color change of gold nanoparticle arrays when annealed at a range of temperatures. We combine spectral measurements with atomic force microscopy (AFM) and scanning electron microscopy (SEM) to investigate how the color change correlates with the alteration of the nanoparticle size or shape.

II. METHOD

A total of six gold nanoparticle arrays were made, following the manufacturing procedure used by Greve *et al.*[17] The samples were labeled A–F. Samples A–E were prepared on $24 \times 24\,\mathrm{mm}^2$ borosilicate glass substrates (Menzel-Gläser). Sample F will be discussed later. After an initial cleaning using acetone, methanol, and isopropanol, the glass substrates were spin-coated with PMMA to a thickness of approximately 190 nm. A 3 nm chromium thin film was deposited on top of the PMMA using Temescal FC-2000 electron beam evaporation (EBE) to make the substrates conductive for electron beam lithography (EBL). Raith eLINE EBL was used for patterning the samples A–E with square arrays of 2 nm pixels. A pattern resulting in holes of approximately 50–80 nm diameter and an interparticle distance of 160 nm was patterned. The interparticle distance was chosen to avoid optical coupling between the MNPs.[18] A total area of $4 \times 4\,\mathrm{mm}^2$ was patterned. The dose was 0.0090 pC per dot, the acceleration voltage was 15 kV, and the beam aperture was 30 μm in diameter, resulting in a beam current of 0.175 nA and a dwell time per pixel of 0.051429 ms. The working distance was approximately 10.7 mm.

After patterning, the chromium was removed using a chromium etchant (Transene chromium etchant 1020). The PMMA exposed by the electron beam was removed by submerging the samples for two minutes in developer (Micro Resist Technology developer mr-Dev 600). Approximately 25 nm gold [estimated using a quartz crystal microbalance (QCM)] was deposited using EBE. In order to avoid undesired optical effects no adhesion promoting layer was used for the gold film. It was still possible to produce large, high quality arrays. Lift off was done by soaking the sample in *N*-methyl-2-pyrrolidone heated to 80 °C for 2 h. This removed the PMMA, leaving only the gold nanoparticles on the substrate. Figure 1 shows SEM images of samples A and D, taken both perpendicularly and tilted at a 45° angle. It has been discussed in the literature that gold does not adhere well to glass substrates, but this was not an issue for the sample preparation and optical experiments presented here. However, it became an issue for the AFM characterization which will be discussed in Sec. II.

Annealing was done in a Nabertherm GmbH (LE2/11/R6) furnace. The furnace operates in air at atmospheric pressure and was preheated to the set temperature before a sample was inserted. Annealing was done for 5 min for each temperature.

To characterize the color change resulting from annealing, a spectral analysis was performed. For samples with little or no scattering, the terms extinction and absorption are interchangeable. The extinction for samples with low reflectance is given as

$$\text{extinction} = -\log(t), \tag{1}$$

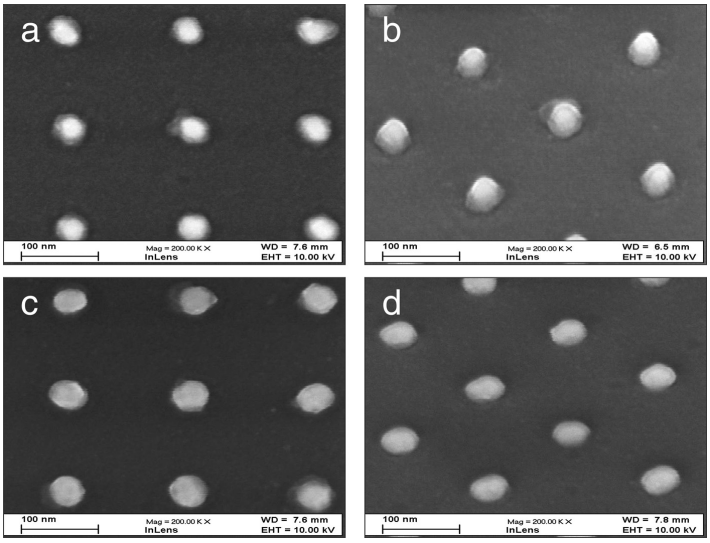

FIG. 1. (a) SEM image of sample A, showing the unannealed square array of gold nanoparticles with 66 nm diameter, 25 nm height, and 160 nm particle distance. (b) SEM image of sample A, taken at a 45° angle. (c) SEM image of sample D, which has been annealed at 450 °C. (d) SEM image of sample D, taken at a 45° angle. The hemispherical shape of the particle can be seen. The samples were coated with 3 nm chromium before imaging.

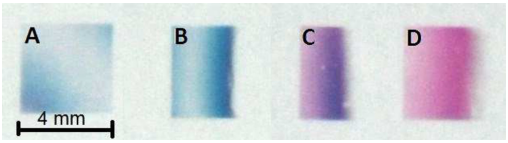

FIG. 2. (Color online) Macroscopic scale optical image of gold nanoparticle arrays. Sample A is not annealed, B is annealed at 150 °C, C at 300 °C, and D at 450 °C.

where t is transmittance through the sample.[1,18] This was measured on samples A–E using a Filmetrics F10-RT thin film analyzer. This instrument has a wavelength range from 380 to 1050 nm. Illumination from a white light source with normal incidence on the sample, and the transmitted spectrum was detected and analyzed using a spectrometer. Each measurement has been background corrected by subtracting the bare glass substrate signal, and five measurements were done for each temperature at random positions within the MNP array. To determine the peak extinction, each spectrum was fitted with a two term Gaussian model using MATLAB. Both Lorentzian[19,20] and Gaussian[21,22] fittings are commonly used in the literature. Macroscopic images of samples A-D were taken using a Nikon D80 digital camera (see Fig. 2).

After the optical measurements had been completed, the samples were coated with 3 nm chromium to avoid charging during the SEM investigation, where the size of the nanoparticles in the respective arrays was determined. Sixteen images were taken, 1.4 mm from all four corners (1 mm from the edges) for each of the $4 \times 4\,\text{mm}^2$ MNP arrays. Every image contains 35 nanoparticles, resulting in 560 nanoparticles imaged for each of the samples A–E. Using IMAGEJ software,[23] the diameter and area was calculated for all the nanoparticles. The results are presented in Table I.

Sample F was designed to be used for detailed AFM and SEM analysis. To avoid charging effects in the SEM images, a $20 \times 20\,\text{mm}^2$ ITO coated glass (about 350 nm thick) with 15–30 Ω/cm resistance was used as the substrate. We cannot exclude that this change in substrate can lead to a change in the interfacial energy between gold and the substrate, thus leading to a change in the wetting behavior of gold on these surfaces. We did notice that it appeared to be slightly easier to scrape off particles from the ITO covered substrate in the AFM. The same PMMA thickness was used for samples A–E, but no chromium layer is needed since the substrate is now conducting. The EBL pattern used was also changed, so that the nanoparticles only cover $30 \times 30\ \mu\text{m}^2$, split into 15 $\times$ 15 arrays, each with 10 $\times$ 10 nanoparticles. Each array was configured with a marker in the form of a selectively missing nanoparticle, so that every array and thereby every nanoparticle is uniquely identifiable. In addition, the nanoparticle arrays are surrounded by an area of $3\,\text{mm}^2$ filled with arrows, 5 or 10 μm in size depending on whether they are closer or further from the arrays than 0.5 mm, respectively. All arrows are pointing in the direction of the nanoparticle arrays and are included to aid in locating the arrays. The arrows were necessary because our AFM (Anfatech "Eddy") does not have built in optics for sample positioning or similar; hence, the arrows were vital for locating the gold nanoparticle arrays. After EBL patterning, the sample was developed, and 35 nm gold was deposited with EBE. A thicker gold layer was used (35 nm) in order to give a larger topographic change for the AFM, where particles are relative to the substrate. The lift-off step is the same as for samples A–E. See Fig. 3 for an overview SEM image of sample F.

AFM characterization of sample F was performed using Anfatech "EDDY" in the Kelvin probe mode (KPFM). KPFM was used because here the scanning probe retains a relatively large distance from the surface and it was found that using both dynamic and contact mode settings resulted in nanoparticles being scraped off the surface. The instrument used a NSC18/Ti-Pt cantilever from Ultrasharp, which has a 3.5 N/m and radius of curvature less than 35 nm. The drive amplitude was set to 2.0 V. Our AFM could not resolve the lateral dimensions of the nanoparticles. Therefore, the AFM is only used for measuring the topological response in

TABLE I. Average and standard deviation values of the diameter and area for samples A–F calculated using IMAGEJ software and SEM images is presented. Five hundred and sixty nanoparticles were measured for each sample (samples A–E). For sample F, the same 99 nanoparticles were measured after each annealing step. Samples A–E has a height of 25 nm, whereas sample F has a height of 35 nm (estimated using a QCM).

Sample	Temp. (°C)	Diameter (nm)	Area (nm^2)
A	0	50 ± 5	1400 ± 200
B	150	59 ± 10	2000 ± 600
C	300	75 ± 8	3400 ± 600
D	450	66 ± 10	2600 ± 700
E	600	50 ± 5	1600 ± 300
F	0	69 ± 7	2700 ± 500
F	150	66 ± 7	2600 ± 500
F	300	67 ± 7	2700 ± 500
F	450	65 ± 6	2700 ± 500

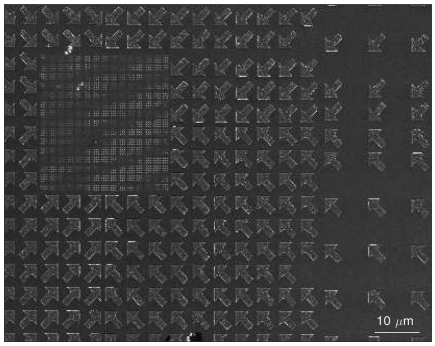

FIG. 3. SEM image of the indexed sample F, with a $30 \times 30\ \mu\text{m}^2$ area covered with gold nanoparticles with 69 nm diameter, 35 nm height, and 160 nm pitch, and surrounded by 5 μm sized arrows. Sample F is used for line profile and area analysis of specific nanoparticles using AFM and SEM. The dark stripes across the arrays are caused by the Moiré effect.

the z-direction. For nanoparticle diameter and area measurements, the SEM images were used. Our AFM instrument does not have any stage positioning mechanism, but by taking an AFM image, and pushing the sample manually with a pair of tweezers in the direction of the pointing arrows in the pattern described above, individual nanoparticles could be repeatedly located. The topographical images were analyzed using the software GWYDDION.[24] First, the images were adjusted for tilt, and then, the nanoparticle profile was investigated by line analysis, both in the vertical and horizontal directions.

SEM characterization of sample F was carried out using an acceleration voltage of 10 kV, the aperture was 30 μm, imaging was done using an InLens detector, and the contrast and brightness was kept the same for all images. Ninety nine nanoparticles were imaged, and the diameter and area of each nanoparticle was extracted using IMAGEJ. For finding the nanoparticle area, the software uses a threshold contrast to determine the edges of each nanoparticle. By counting the number of pixels within the nanoparticle, and using the correct pixel to nm^2 ratio, the area of the nanoparticle was determined. The diameter was found as a statistical average obtained by rotating the nanoparticle 360° with 2° increments. The results of the image analysis are presented in Table I.

III. RESULTS AND ANALYSIS

Figure 2 shows the macroscopically observed effect of annealing. The samples appear to turn red when annealed because more of the blue light is absorbed (the extinction peak blue-shifts). All samples A–E looked identical to the naked eye before annealing with respect to the color.

The extinction spectra for samples A–E for the different annealing steps are presented in Fig. 4(a). Sample A was not annealed, B was annealed at 50, 100, and 150 °C, C at 200, 250, and 300 °C, D at 350, 400, and 450 °C, and E at 500, 550, and 600 °C. Spectra were taken for each sample before they were annealed and are included as the top five extinction spectra in Fig. 4(a), and as the extinction peak data points at 20 °C in Fig. 4(b). The extinction peak became narrower with annealing, shrinking from 500 to 150 nm FWHM. The peak position (derived from a two term Gaussian fit) is plotted against the annealing temperature in Fig. 4(b). The uncertainty given here is the root mean square error of the Gaussian fit. As can be seen, all samples had extinction peaks between 570 and 580 nm before annealing, and the extinction peak shifted from 580 to 520 nm as the annealing temperature increased to 450 °C, followed by a light red-shift of a few nm up to 600 °C. The shift in extinction peak can be seen to be not so closely linked to the size of the nanoparticles, as the effect is very consistent, even with rather large nanoparticle size variation between 50 and 75 nm for samples A–E.

To investigate the relationship between the optical effect and the appearance of the nanoparticles, a total of 99 nanoparticles on sample F were imaged by SEM and AFM before annealing, and for annealing temperatures of 150, 300, and 450 °C. As discussed earlier, SEM and AFM imaging was done for exactly the same 99 nanoparticles. The combined AFM and SEM images allow us to obtain more information about the sample appearance. The results are presented in Fig. 5 and Table I. The technique for measuring the topographical response with the Kelvin probe is identical to that of the dynamic mode AFM. However, the additional tip bias and the fact that our sample is not grounded can result in charging effects in the image. The measured topographical response of the nanoparticles decrease from nominally 36 ± 3 to 26 ± 3 nm for annealing up to 450 °C. However, it is not certain that this is due to a true height change. It appears more likely that this is caused by a more strongly varying response in the unannealed nanoparticles, due to them being rougher. The measurements suggest that the nanoparticle surfaces get smoother with annealing and that the corners get less sharply defined, indicating a transition from the starting cylindrical shape to a more hemispherical

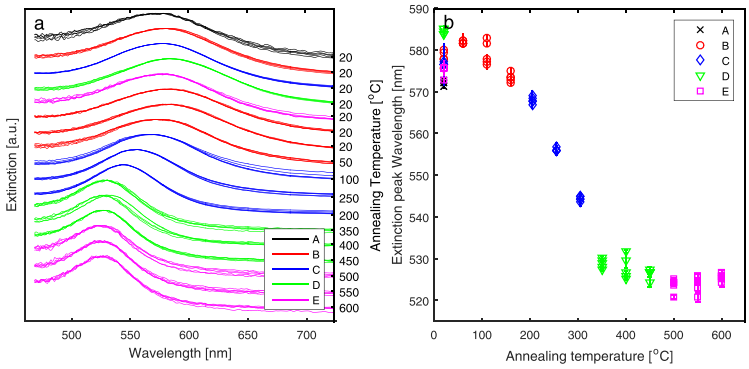

FIG. 4. (Color online) (a) Extinction spectra for gold nanoparticles samples A–E. The spectra are normalized and offset from each other for clarity. (b) Extinction peak position for gold nanoparticles done at annealing temperatures ranging up to 600 °C. As annealing temperature increases, the extinction peak blue-shifts. Macroscopically, this will cause the array to appear red because more of the blue light is absorbed.

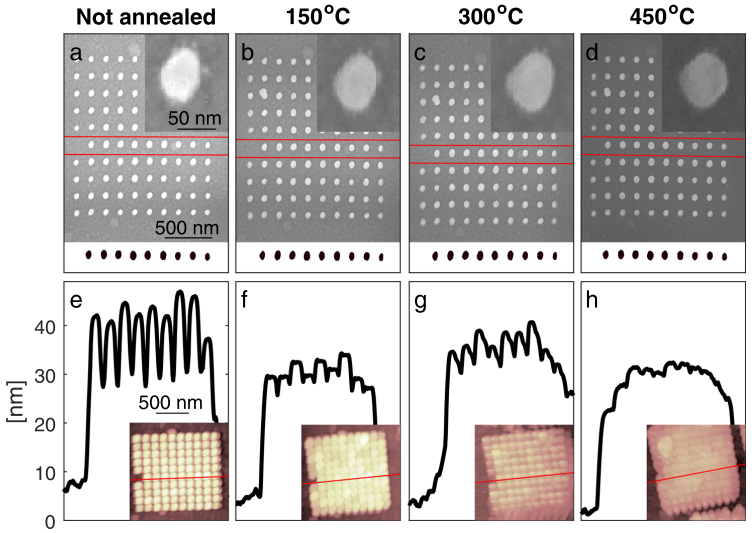

FIG. 5. (Color online) (a)–(d) SEM image of sample F gold nanpoarticles. Upper right inset shows the leftmost particle between the red lines, magnified. Bottom inset shows area analysis of nanoparticles between the red lines. (e)–(h) AFM line analysis taken over the same nanoparticles as the SEM area analysis. Inset show AFM image with red line indicating where the line profile is taken from. Images are taken before annealing [(a) and (e)], and after annealing at 150 °C [(b) and (f)], 300 °C [(c) and (g)], and 450 °C [(d) and (h)]. All the images are taken of the same nanoparticles. Note that due to the small arrays a slight dose variation can be seen (due to proximity effects), visible as a slight size variation from center to edge of the nanoparticle array.

shape. As can be seen from the SEM images and the area measurements presented in Table I, there does not appear to be a change in the area of the nanoparticles. We quantified the smoothening effect by using the SEM images to compare the perimeter length, also obtained from IMAGEJ analysis, to the circumference of a hypothetical smooth circle using an average radius calculated from the area data. We see that the surface root mean square roughness decreased from approximately 1.6 to 1.0 nm (estimation is sensitive to image resolution), a decrease of 35%, after annealing at 450 °C for the same sample. This is quantitatively in line with the predictions of Kessentini *et al.*[14] It is interesting that the effect seems to be so strong given the relatively low annealing temperatures. Considering the manufacturing process for samples A–F which would produce cylinders, it is plausible that the shape of our nanoparticles, initially cylindrical would become more hemispherical upon annealing. This would contribute to an even stronger blue-shift.[15,16]

In Fig. 1, the gold nanoparticles appear to have facets at their edges. The facets may indicate some level of crystallinity. Bosman *et al.*[7] show that annealing may increase the crystallinity of gold nanostructures, at least if it is low at first. It is not possible to say for certain if this occurs in our samples. The inset in Fig. 5(a) shows sub-10-nm particles near the edges. These particles come most likely from evaporated gold during EBE. The PMMA mask has an undercut, allowing room for stray gold to attach to the substrate near the gold particle edges. From Figs. 5(a)–5(d), we see an indication that some of these sub-10-nm particles appear to be consumed by the larger particle when annealed. This process seems to have no impact on the diameter or area of the particles (see Table I). A FDTD LUMERICAL[25] simulation of a 50 nm gold nanoparticle placed on glass with two 5 nm particles placed 5 nm from the larger nanoparticle reveals that the presence of sub-10-nm particles increases the amplitude and FWHM of the extinction peak slightly, but does not change the peak position. This is consistent with the decrease in FWHM observed in Fig. 4(a), as the sub-10-nm particles are consumed by the nanoparticle when annealed.

Karakouz *et al.*[10] reports that gold islands start sinking into a glass substrate at 550–600 °C. We observe the blue-shift in the extinction peak at lower temperatures. However, the slight red-shift occurring between 500 and 600 °C seen in Fig. 4 can potentially be attributed to this effect, as sinking into the substrate would not only change the surrounding medium, but in a sense also make the particles shorter relative to the substrate, which would cause a red-shift.[11,12] Borosilicate glass does not change refractive index significantly over the temperature range used in this experiment.[26]

IV. CONCLUSION

In this paper, we present optical measurements of gold nanoparticle arrays which change color when annealed up to 600 °C. The extinction peak blue-shifts from 580 to 520 nm already after annealing to 450 °C, after which a weak red-shift is observed. The visual appearance of the nanoparticles changes from blue to red. We conclude that the shift of 60 nm is mainly caused by two factors: first, a smoothening of the nanoparticle surface which is observed in SEM and

AFM images; second, we hypothesize a rounding of corners in the original cylindrical shape. Both of these effects would cause a blue-shift according to theoretical predictions. The final red-shift can be contributed to the nanoparticles starting to sink into the substrate. Our results demonstrate that seemingly minor changes in the metal nanoparticle appearance can lead to a strong change in the LSPR effect. We suggest that nanoparticle arrays, implanted in various devices, for example, using nanoimprint, could have potential applications for controlling the temperature product history (i.e., as a test to ensure that the temperature was never above a certain limit). The fact that the effect of temperature exposure is irreversible for these nanoparticle arrays and can be observed with the naked eye without any need of electronic readout or power supply is particularly advantageous.

ACKNOWLEDGMENTS

The authors thank Anne-Dorothea Müller, Anfatec Instruments AG for fruitful discussions. This work was carried out in the UiB Nanostructures laboratory funded by Trond Mohn, Bergen Research Foundation and the Norwegian Research Council.

[1]S. A. Maier, *Plasmonics: Fundamentals and Applications* (Springer, New York, 2007).
[2]X. Xiang, X. T. Zu, S. Zhu, C. F. Zhang, and L. M. Wang, Nucl. Instrum. Method B **250**, 229 (2006).
[3]P. Xiao-Niu, L. Min, Y. Liao, Z. Xian, and Z. Li, Chin. Phys. Lett. **25**, 4171 (2008).
[4]K. Chan, B. T. Goh, S. A. Rahman, M. R. Muhamad, C. F. Dee, and Z. Aspanut, Vacuum **86**, 1367 (2012).
[5]Z. W. Lei, M. Liu, W. Ge, Z. P. Fu, K. Reinhardt, R. J. Knize, and Y. Lu, Appl. Phys. Lett. **101**, 083903 (2012).
[6]K. Omri, A. Bettaibi, I. Najeh, S. Rabaoui, K. Khirouni, and L. El Mir, J. Mater. Sci.: Mater. Electron. **27**, 226 (2016).
[7]M. Bosman, L. Zhang, H. D. ans Shu Fen Tan, C. A. Nijhuis, C. Qiu, and J. K. W. Yang, Sci. Rep. **4**, 5537 (2014).
[8]W. Cai, H. Hofmeister, T. Rainer, and W. Chen, J. Nanopart. Res. **3**, 441 (2001).
[9]H. Bi, W. Cai, L. Zhang, D. Martin, and F. Träger, Appl. Phys. Lett. **81**, 5222 (2002).
[10]T. Karakouz, A. B. Tesler, T. A. Bendikov, A. Vaskevich, and I. Rubinstein, Adv. Mater. **20**, 3893 (2008).
[11]Y. M. Bae, K.-H. Lee, J. Yang, and D. Heo, J. Nanomater. **2014**, 175670.
[12]T. R. Jensen, M. D. Malinsky, C. L. Haynes, and R. P. Van Duyne, J. Phys. Chem. B **104**, 10549 (2000).
[13]J. C. Hulteen, C. J. Patrissi, D. L. Miner, E. R. Crosthwait, E. B. Oberhauser, and C. R. Martin, J. Phys. Chem. B **101**, 7727 (1997).
[14]S. Kessentini and D. Barchiesi, *State of the Art in Biosensors – General Aspects*, edited by Dr. T Rinken (InTech, Croatia, 2013), p. 311.
[15]J. Qian, C. Liu, W. Wang, J. Chen, Y. Li, J. Xu, and Q. Sun, Plasmonics **8**, 955 (2013).
[16]M. Liu, P. Guyot-Sionnest, T.-W. Lee, and S. K. Gray, Phys. Rev. B **76**, 235428 (2007).
[17]M. M. Greve, T. O. Håvardstun, and B. Holst, J. Vac. Sci. Technol., B **31**, 06F410 (2013).
[18]W. Rechberger, A. Hohenau, A. Leitner, J. Krenn, B. Lamprecht, and F. Aussenegg, Opt. Commun. **220**, 137 (2003).
[19]M. A. Schmidt, D. Y. Lei, L. Wondraczek, V. Nazaba, and S. A. Maier, Nat. Commun. **3**, 1108 (2012).
[20]G. Vecchi, V. Giannini, and J. Gómez Rivas, Phys Rev. B **80**, 201401(R) (2009).
[21]C. Diaz-Egea, W. Sigle, P. A. van Aken, and S. I. Molina, Nanoscale Res. Lett. **8**, 337 (2013).
[22]L. Soares, A. Csaki, J. Jatschka, W. Fritzsche, O. Flores, R. Franco, and E. Pereira, Analyst **139**, 4964 (2014).
[23]"IMAGEJ," https://imagej.nih.gov/ij/ (accessed 21 June 2016).
[24]"GWYDDION," http://gwyddion.net/ (accessed 21 June 2016).
[25]"LUMERICAL," https://www.lumerical.com/ (accessed 31 August 2016).
[26]N. Ritland, J. Am. Ceram. Soc. **39**, 403 (1956).